Materials Transactions, Vol. 49, No. 6 (2008) pp. 1278 to 1283

Dislocation Bow-Out Model for Yield Stress of Ultra-Fine Grained Materials

Masaharu Kato[1], Toshiyuki Fujii[2] and Susumu Onaka[1]

[1]*Department of Materials Science and Engineering, Interdisciplinary Graduate School of Science and Engineering, Tokyo Institute of Technology, Yokohama 226-8502, Japan*
[2]*Department of Innovative and Engineered Materials, Interdisciplinary Graduate School of Science and Engineering, Tokyo Institute of Technology, Yokohama 226-8502, Japan*

A dislocation bow-out model has been developed to explain the strength of ultra-fine grained (UFG) materials with grain size roughly between 20 nm to 500 nm. In the model, perfect dislocations are assumed to be nucleated at grain-boundary sources and bow out between two pinning points on a boundary. Yielding is considered to occur when a dislocation takes a semi-circular shape under applied stress. Statistical consideration is introduced to evaluate the most probable pinning-point distance as a function of grain size. Comparison with experimental results is made for fcc UFG metals. It is found that yield stress as well as thermal activation parameters can be explained reasonably by the present theoretical model. [doi:10.2320/matertrans.MRA2008012]

(Received January 9, 2008; Accepted March 12, 2008; Published May 1, 2008)

Keywords: *strength, ultra-fine grained materials, deformation mechanism, yield stress, grain boundaries, dislocation, modeling*

1. Introduction

Plastic deformation characteristics of ultra-fine grained (UFG) and nano-cystalline (NC) materials have been paid much attention. Cheng *et al.* classified the deformation mechanisms of UFG and NC materials into four different regimes.[1)] They have called the smallest grain-size regime as "Nano-1" for grain sizes smaller than, say, 10 nm. In this regime, plastic deformation occurs by grain-boundary processes, such as grain-boundary sliding or Coble creep. Dislocation activities are not important here. It is in this regime that the so-called inverse Hall-Petch (H-P) relation or H-P breakdown for grain-boundary strengthening is often observed.[2–11)]

As grain size becomes larger than about 10 nm, *i.e.*, in the "Nano-2" regime, grains are sheared by twinning or by Shockley partial dislocations, leaving stacking faults behind them. Since the partial dislocations have smaller Burgers vector than that of perfect dislocations, they can bow out and move more easily than the perfect dislocations under smaller applied stresses.[12–14)] The third regime is defined as the "UFG" regime and starts with grain size larger than about 20 nm for Ni[14)] and 20 to 35 nm for Al.[1,15,16)] In this regime, lattice dislocations are nucleated in grain boundaries, and shear the grains. Even when the stacking fault energy is small, a trailing partial can be nucleated before the entire grain is sheared by a leading partial. Therefore, the plastic deformation in the UFG regime occurs by the motion of perfect dislocations that are emitted from the grain-boundary sources. Lastly comes the fourth "Traditional" regime when the grain size becomes larger than several-hundred nanometers to 1 μm, depending on the material. Here, many in-grain as well as grain-boundary dislocation sources become available to produce plastic deformation, and "normal" metal behaviour is expected.

In the present study, we will focus on the UFG regime with grain diameter d roughly between 20 nm to 500 nm. Many theoretical models on the strength of the UFG materials have been developed and most of them incorporate the H-P-type $d^{-1/2}$ dependence of the critical resolved shear stress (CRSS) into the models.[9,17–23)] For theories that do not directly deal with the H-P relation, grain boundaries are regarded to be potential dislocation sources[24–26)] and the bow-out of a dislocation from a grain-boundary source is considered to determine the CRSS.[1,5,27)] Pinning points for the dislocation bow-out lie on a slip plane at a grain boundary and act as obstacles against dislocation motion. They may be boundary ledges, triple points or segregated impurity atoms. Such dislocation bow-out models naturally predict the d^{-1} dependence of strength and the resultant CRSS may be too large to explain experimental values.[12–14,28)]

Scattergood and Koch[5)] have suggested that dislocations in UFG and NC materials should not create long-range elastic fields around them. The grain boundaries are generally regarded to be incoherent and screen the elastic fields around a dislocation. Therefore, the outer cutoff distance of the dislocation elastic field becomes at most d.[5)] If this fact is taken into account, discussion can be modified to predict lower CRSS values than those expected from the traditional d^{-1} dependence.[1,27)] In the present study, we will follow this idea to estimate the yield stress of UFG materials.

As mentioned above, when dislocations are emitted from grain boundary sources, they bow out between boundary pinning points and CRSS is identified as the stress necessary for a dislocation to bow out to a semi-circular shape. Then, the local bowed-out segment of the dislocation should have the self energy and line tension that are even smaller than those predicted by Scattergood and Koch. In fact, to express the energy of a looped or semi-circular dislocation, the outer cutoff length in the logarithmic term of the self energy is often evaluated to be equal to the radius of the dislocation curvature.[29–31)]

In the present study, the main focus will be placed upon the proposal of a strengthening mechanism in the UFG regime with grain size roughly between 20 nm to 500 nm. As mentioned above, perfect dislocations emitted from grain boundaries are considered to travel though the whole grain to cause plastic deformation.

2. Theoretical Model

2.1 Line tension and critical resolved shear stress

Hereafter, we will consider the case that the grain size of UFG materials is small enough so that in-grain dislocation sources are practically absent and only grain-boundary sources are active. The line tension T_L of the perfect dislocation is written using the string model as

$$T_L = \frac{\mu b^2}{4\pi} \ln\left(\frac{R}{r_0}\right) = \frac{\mu b^2}{4\pi} \ln\left(\frac{L}{2r_0}\right), \quad (1)$$

where μ is the elastic modulus, b the magnitude of the Burgers vector, R the outer cutoff radius and r_0 the inner cutoff radius representing the dislocation core size. The dislocation character (screw or edge) will not be taken into account in the present analysis. As mentioned in Introduction, to obtain the last term, the outer cutoff R has been set equal to the radius of the dislocation curvature, *i.e.*, $R = L/2$, where L is the distance between pinning points (or the dislocation source length) at grain boundaries. Scattergood and Koch have shown that their bow-out model can explain experimental results reasonably when r_0 is taken in the range $2b \le r_0 \le 10b$.[5] Therefore, we will assign $r_0 = 5b$ in the present study. Then, eq. (1) can be rewritten as

$$T_L = \frac{\mu b^2}{4\pi} \ln\left(\frac{L}{10b}\right) \quad (2)$$

From eq. (2), the CRSS τ_c is determined by the stress necessary for the dislocation to bow out in a semi-circular shape from the grain boundary as

$$\tau_c = \frac{T_L}{b(L/2)} = \frac{\mu b}{2\pi L} \ln\left(\frac{L}{10b}\right), \quad (3)$$

Cheng *et al.*[5] have adopted a similar but more detailed expression of the CRSS derived by Hirth and Lothe.[31] Their eq. (1) for edge dislocations is written in our notations as

$$\tau_c = \frac{\mu b}{2\pi L(1-\nu)} \left\{ \left(1 - \frac{3}{2}\nu\right) \ln\left(\frac{L}{b}\right) - 1 + \frac{1}{2}\nu \right\}, \quad (4)$$

where ν is the Poisson ratio. Assuming $b = 0.3\,\text{nm}$ and $\nu = 0.3$, the values of τ_c calculated from eqs. (3) and (4) were compared. It was found that they differ by at most 15% within a wide range of $15\,\text{nm} \le L \le 10\,\mu\text{m}$. Therefore, for all practical purposes, eq. (3) is much simpler but as good an expression as eq. (4). This again justifies the assignment of $r_0 = 5b$ in this study.

2.2 Source length at grain boundaries

It should be noted that τ_c in eq. (3) cannot exceed the theoretical shear strength of about $\mu/30$. Examination using various representative values for constants reveals that this is always assured for eq. (3). On the other hand, if the conventional expression of the Orowan stress $\tau_{OR} = \mu b/L$ is adopted, the condition of $\tau_{OR} \le \mu/30$ is satisfied for $L \ge 30b$. Therefore, the lower bound of L is roughly estimated as 10 nm for many metals with $b \approx 0.3\,\text{nm}$. Since L cannot exceed the grain size d, the source length, or the distance between the grain-boundary pinning points, lies within the range

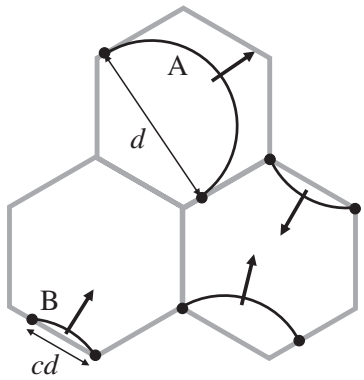

Fig. 1 Bowing out of dislocations emitted from grain-boundary sources under an applied stress τ. The dots indicate the pinning points.

$$\lambda \le L \le d, \quad (5)$$

with $\lambda = 10\,\text{nm}$. It is true that this assignment of $\lambda = 10\,\text{nm}$ is rather conventional. However, as will be shown in section 2.4, the present discussion does not strongly depend on the chosen length of λ.

2.3 Statistical distribution of pinning points

Figure 1 shows the bowing out of perfect dislocations emitted from grain-boundary sources when a shear stress τ is applied in the material. If the distance between pinning points is large, such as A in Fig. 1, the dislocation can bow out in a semi-circular shape and τ becomes the CRSS for the long-range movement of the A dislocation. On the other hand, if the pinning-point distance is small such as B, only a small bow-out is possible and a larger stress is necessary before the B dislocation can take a semi-circular shape.

Statistically speaking, the source length L that obeys the condition (5) is randomly distributed on grain boundaries and is a fraction of the grain diameter d so that $L = cd$, where c is positive and does not exceed unity. Therefore, we can assume that any pinning-point distance L, or any value of c, satisfying the above condition (5) is equally possible; the larger L causes smaller τ_c.

If the average source length $\langle L \rangle$ is found as a function of d, insertion of this $\langle L \rangle$ into L in eq. (3) should give the most probable CRSS for a given d. Then, the problem now is to find the value $\langle L \rangle$. This can be done using statistics as follows.

Let us approximate $n \approx d/\lambda$ as an integer representing the number of potential pinning-point sites at an intersection between a grain boundary and a slip plane. We have

$$L = cd = cn\lambda, \quad 0 < c < 1. \quad (6)$$

As a simple example, we will first consider the case where equally-spaced (with separation λ) four (4) potential pinning point sites exist at an intersection line between a grain boundary and a slip plane, as shown in Fig. 2. When a dislocation bows out between any two of the four sites, there are

$${}_4C_2 = \frac{4!}{2!(4-2)!} = 6 \quad (7)$$

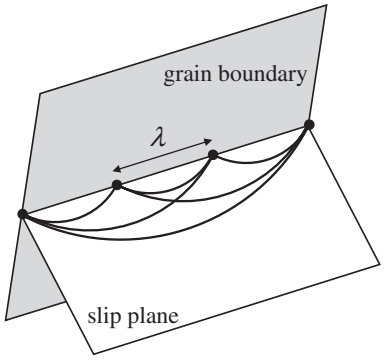

Fig. 2 Equally-separated four pinning points at an intersection between a grain-boundary plane and a slip plane.

different ways to choose the two pinning points. Among them, one has the distance 3λ, two have 2λ and three have λ. Since these six choices are assumed to occur with equal probabilities, the average separation $\langle L\rangle$ between the pinning points is calculated as

$$\langle L\rangle = \frac{(3\times\lambda)+(2\times 2\lambda)+(1\times 3\lambda)}{{}_4C_2} = \frac{5}{3}\lambda. \qquad (8)$$

This analysis can be generalized easily for a grain size of $d = n\lambda$ and the average separation $\langle L\rangle$ and average coefficient $\langle c\rangle$ of c are obtained as

$$\langle L\rangle = \frac{n\lambda+(n-1)2\lambda+(n-2)3\lambda+\ldots+1\cdot n\lambda}{{}_nC_2} = \frac{n+2}{3}\lambda = \frac{d+2\lambda}{3}, \qquad (9)$$

$$\langle c\rangle = \frac{\langle L\rangle}{d} = \frac{n+2}{3n} = \frac{1+2(\lambda/d)}{3}. \qquad (10)$$

The number of grains in a usual UFG tensile specimen is extremely large. In such a case, the average value $\langle L\rangle$ in eq. (9) is statistically interpreted as the most probable separation between the pinning points. For readers of interest, the statistical interpretation is shown in Appendix.

2.4 Yield stress

From eqs. (3) and (9) together with the Taylor factor $M = 3.06$, the tensile yield stress σ_y of fcc metals is expressed as

$$\sigma_y = M\tau_c = \frac{3M\mu b}{2\pi(d+2\lambda)}\ln\left(\frac{d+2\lambda}{30b}\right) \approx \frac{3\mu b}{2(d+2\lambda)}\ln\left(\frac{d+2\lambda}{30b}\right). \qquad (11)$$

Here, the approximation of $M/\pi \approx 1$ is adopted to obtain the last term. Since all the quantities in eq. (11) are either known or already assigned above ($\lambda = 10$ nm), we can calculate the values of σ_y and compare them with those obtained in previous experiments. Trial calculations of eq. (11) for $b = 0.3$ nm and $20\,\text{nm} < d < 500\,\text{nm}$ revealed that wide variation of λ from 2 nm to 20 nm caused only less than 15% change in the σ_y values. Therefore, we can safely assign $\lambda = 10$ nm for eq. (11) to compare the predicted yield stress with experimental values.

3. Comparison with Previous Studies

3.1 Yield stress

Figures 3, 4 and 5 show the H-P plots of predicted yield stress σ_y from eq. (11) and the experimental data available in the literature for Ni,[10,11,32] Cu[13,19,33,34] and Al,[35–37] respectively. Constants in eq. (11) used to calculate σ_y are listed in Table 1. Assuming that the yield stress for single crystals of the fcc metals are negligibly small, eq. (11) was used without any additional terms. We can immediately notice from Figs. 3 to 5 that the theoretical curves well reproduce the H-P behaviour at larger grain sizes. The agreement between the model predictions and experimental

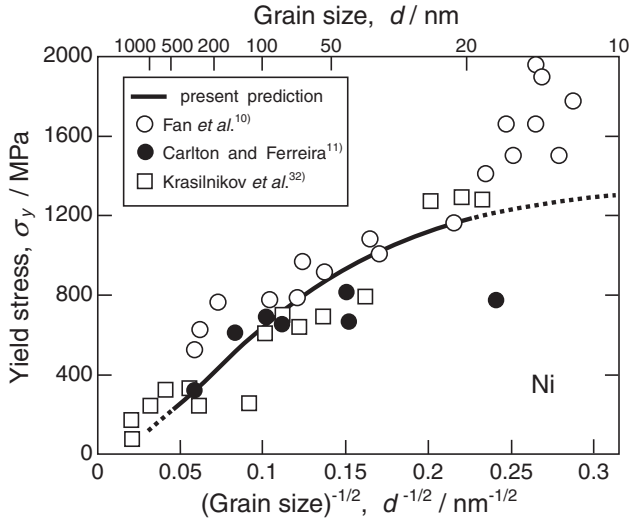

Fig. 3 Yield stress σ_y as a function of the inverse square root of the grain size d in Ni. The solid line shows the model prediction of the present study and circles (tensile tests) and squares (hardness tests) are experimental data available in the literature.[10,11,32] The hardness values H_v were converted to the yield stress values σ_y using the usual relation $H_v = 3\sigma_y$.

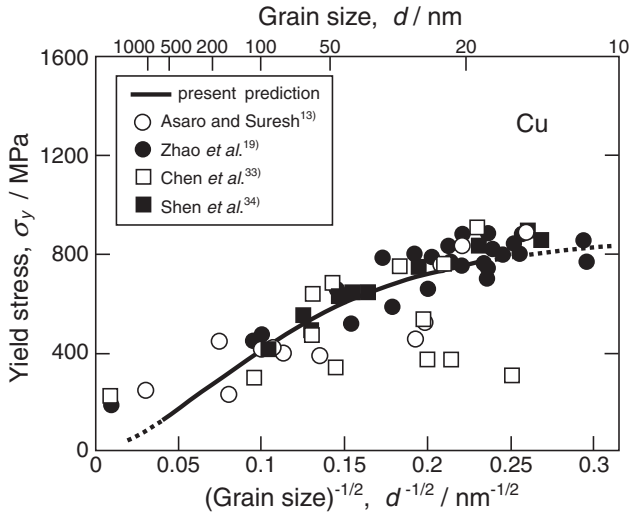

Fig. 4 Yield stress σ_y as a function of the inverse square root of the grain size d in Cu. The solid line shows the model prediction of the present study and circles and squares are experimental data available in the literature.[13,19,33,34] Nano-scale twin lamella spacing instead of grain size are plotted as the horizontal axis for the data by Shen *et al.*[34]

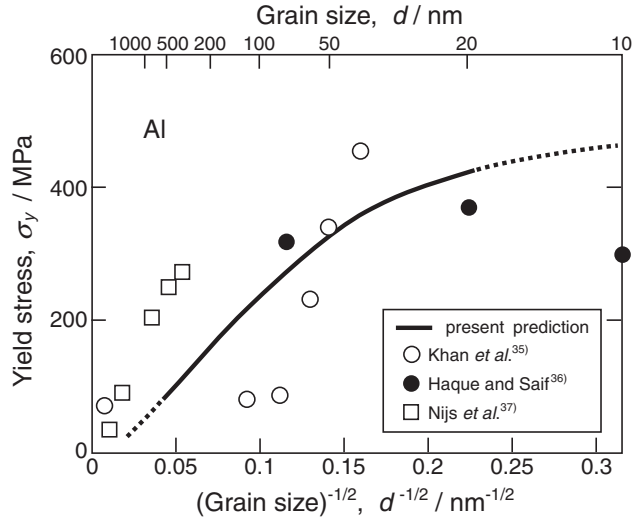

Fig. 5 Yield stress σ_y as a function of the inverse square root of the grain size d in Al. The solid line shows the model prediction of the present study and circles are experimental data available in the literature.[35–37] The data by Nijs *et al.*[37] are for an Al-Mg alloy.

Table 1 Values for constants used to calculate σ_y from eq. (11).

	Ni	Cu	Al
Shear modulus, μ/GPa	76	48	26
Burgers vector, b/nm	0.249	0.255	0.284
Source length, λ/nm	10	10	10

data are also reasonably well, at least no worse than any other existing models can predict aside from the empirical H-P straight line. Although the data points for Ni deviate from the theoretical curve for grain sizes smaller than about 20 nm, this is considered to be natural since our model can be applied to the UFG regime of grain size roughly between 20 nm to 500 nm, as mentioned previously.

A similar dislocation bow-out model has been used by Scattergood and Koch to explain the so-called inverse H-P relation.[5] As explained earlier, they have adopted the grain size d as the outer cutoff length in the logarithmic term in eq. (1). In the present study, usage of eq. (11) causes a shift in the peak stress towards smaller grain size regions, resulting in the absence of the inverse H-P relation in Figs. 3 to 5. Cheng *et al.* on the other hand, have treated the source length $L = cd$ in eq. (6) as an adjustable parameter.[1] As c becomes larger, the inverse H-P behaviour becomes less significant. They have argued that the source length should become a smaller fraction of the grain size as the grain size increases. However, they could not discuss any further the dependence of c on the grain size. In the present study, on the contrary, the grain-size dependence of c was statistically and analytically incorporated, as shown in eq. (10).

3.2 Strain-rate sensitivity and activation volume

It is well known in fcc NC and UFG materials that strain-rate sensitivity exponent m defined as

$$m \equiv \left(\frac{\partial \ln \sigma}{\partial \ln \dot{\varepsilon}}\right)_T = \frac{1}{\sigma}\left(\frac{\partial \sigma}{\partial \ln \dot{\varepsilon}}\right)_T, \tag{12}$$

increases as grain size becomes smaller.[20,22,29,38–46] Here, σ is the flow stress, $\dot{\varepsilon}$ the strain rate and T the temperature. Typical values of m at grain sizes $d = 20$–30 nm are $m =$ 0.03 to 0.04 for Cu[20,21,28,33,41] and 0.01 to 0.02 for Ni.[43,45,46] Since these values are still too small for grain-boundary sliding ($m = 0.5$) or Coble creep ($m = 1$), these grain-boundary phenomena are unlikely to be the rate-controlling processes in the UFG regime unless strain rate is very small and/or temperature is high.[20,21,34,41,46] Instead, thermally activated dislocation motion to overcome short-range obstacles is considered to be more probable in the UFG regime and some possible mechanisms have been proposed. For example, we find in a recent overview by Dao *et al.*[28] such possible mechanisms as punching of a mobile dislocation through a dense bundle of excess grain-boundary dislocations, defect-assisted dislocation nucleation, de-pinning of a dislocation that is pinned at boundary obstacles, etc. All of these mechanisms must also explain a small activation volume in NC and UFG materials as well as the temperature dependence of strength.

As an additional analysis, let us examine what can be said for the thermally activated dislocation process using the present model. The activation volume v^* is written as

$$v^* \equiv kT\left(\frac{\partial \ln \dot{\gamma}}{\partial \tau}\right)_T = M\,kT\left(\frac{\partial \ln \dot{\varepsilon}}{\partial \sigma}\right)_T = M\,v_\sigma^*, \tag{13}$$

where kT has its usual meaning, $\dot{\gamma}$ the shear strain rate, τ the resolved shear stress and v_σ^* the measured activation volume during plastic deformation under uniaxial stress σ. From eqs. (12) and (13), we have

$$v^* = \frac{M\,kT}{m\sigma}. \tag{14}$$

The physical meaning of v^* is the activation area s^* times the Burgers vector b:

$$v^* \equiv s^* b = l^* d^* b, \tag{15}$$

where l^* is the length of a dislocation that contributes to a thermal activation event for overcoming a short-range obstacle and d^* is the activation distance that scales with the size of the obstacle.

Figure 6 shows a dislocation A that is about to bow out in a semi-circular shape between two pinning points P and Q with separation L. If a thermal activation event occurs locally to overcome the obstacle P, the dislocation A is un-pinned and moves to the position B. Once the configuration B is realized, the curvature of the dislocation A decreases and the long-range motion of the dislocation becomes possible, say, through C and even further. The activation area associated with this unpinning event is defined as the area between the dislocations A and B and is roughly estimated as $s^* \approx \{(L/2) \times b\}/2 = Lb/4$. Therefore, we have

$$v^* = s^* b = Lb^2/4 = (d + 2\lambda)b^2/12, \tag{16}$$

where the average pinning-point separation $\langle L \rangle$ in eq. (9) is substituted for L to obtain the last term. From eq. (16) together with $\lambda = 10$ nm, as assumed in section 2.2, we

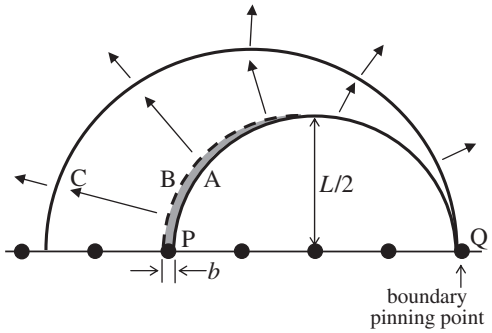

Fig. 6 When the bowing-out dislocation A pinned at boundary obstacles P and Q overcomes the obstacle P by thermal activation, the dislocation A moves locally to B. Then, the dislocation can automatically move to C and further to cause long-range motion. The activation volume for this event is defined as Bergers vector times the activation area bounded by dislocations A and B.

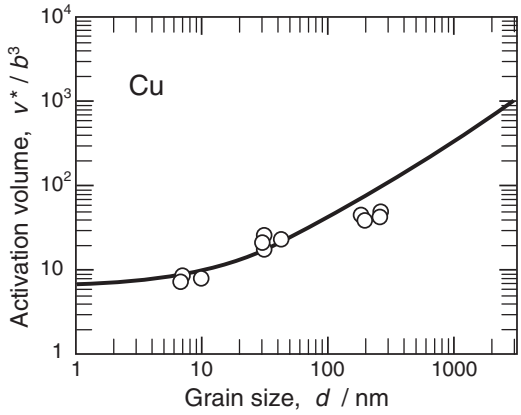

Fig. 7 Predicted grain size dependence of the activation energy of UFG Cu calculated from eq. (16). The data points are taken from the paper by Chen *et al.*[33]

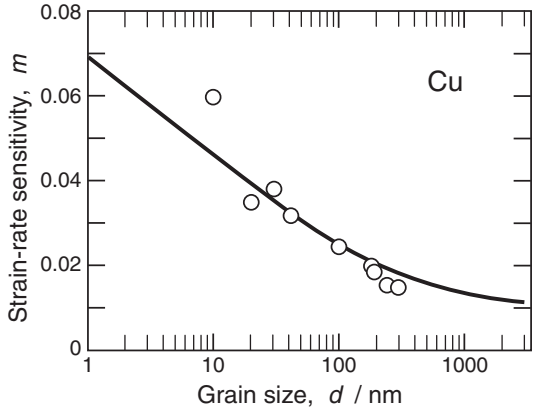

Fig. 8 Predicted grain size dependence of the strain-rate sensitivity of UFG Cu calculated from eqs. (11), (14) and (16). The data points are taken from the paper by Chen *et al.*[33]

can obtain the grain-size dependence of the activation volume. The curve in Fig. 7 shows the calculated activation volume as a function of grain size for Cu. The data points (circles) in the figure were taken from the experimental results summarized by Chen *et al.*[33] As can be seen, the agreement between the theory and experiment is excellent.

A similar plot for m is possible by using eqs. (11), (14) and (16), as shown in Fig. 8. To draw the curve, $M = \sqrt{3}$ was assigned in eq. (14). This assignment is merely for the purpose of comparison with the experimental results (circles in Fig. 8) summarized by Chen *et al.*[33] who used $M = \sqrt{3}$ in their analysis. We again find the excellent agreement.

4. Concluding Remarks

From the present study, we have found that the dislocation bow-out model can reasonably explain not only the observed strength but also the grain-size dependence of the activation volume and strain-rate sensitivity. During the course of this study, the H-P relation was not used nor postulated. This may indicate that the observed H-P relation is just fortuitous and it is not a prerequisite for the deformation mechanism of NC and UFG materials. Further study is necessary to reveal the grain boundary contribution to the strength.

Our discussion on the thermally activated dislocation motion in Section 3.2 is incomplete in a sense that the original equation of strength (eq. (11)) was derived without taking into account the kinetics of deformation. Even if the present de-pinning process does determine the strain-rate sensitivity of UFG materials, a thermal activation event at a given temperature should occur before a dislocation takes a semi-circular shape. Therefore, more rigorous discussion based on the kinetics of plastic deformation is needed. Nevertheless, it is interesting to find that the present study can explain the observed dependencies of strain-rate sensitivity and activation volume on grain size. We believe research along this line will reveal whether or not the present analysis is really applicable as a strength mechanism of the UFG materials.

Acknowlegment

This research was supported by a Grant-in-Aid for Scientific Research on Priority Areas (18062002) by the Ministry of Education, Culture, Sports, Science and Technology of Japan.

Appendix

Let $L\ (= \lambda, 2\lambda, 3\lambda, \ldots, n\lambda)$ be a random variable and its distribution function be described as $P(L)$. For our problem of grain size $d = n\lambda$, L is the group of all the possible source length and $P(L)$ means its frequency of appearance, as shown in Fig. A·1. When $\langle L \rangle$ denotes the average (expectation) of L, we have from eq. (9)

$$\langle L \rangle = (n+2)\lambda/3. \tag{A·1}$$

On the other hand, the variance σ^2 of $P(L)$ is defined as[47]

$$\sigma^2 \equiv \langle (L - \langle L \rangle)^2 \rangle = \langle L^2 \rangle - \langle L \rangle^2. \tag{A·2}$$

Since

$$\langle L^2 \rangle = \frac{2\lambda^2}{n(n+1)} [1^2 \cdot n + 2^2 \cdot (n-1) + 3^2 \cdot (n-2) + \ldots + n^2 \cdot \{n - (n-1)\}]$$

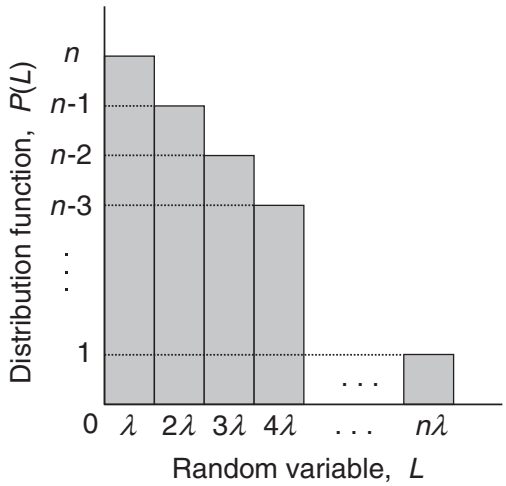

Fig. A·1 Distribution function $P(L)$ of a random variable L representing the source length. The variable L takes values of $\lambda, 2\lambda, 3\lambda, \ldots$ and $n\lambda$ with its frequency of appearance $n, n-1, n-2, \ldots$ and 1, respectively.

$$= \frac{2\lambda^2}{n(n+1)}\left[n\sum_{k=1}^{n}k^2 - \sum_{k=1}^{n-1}k(k+1)^2\right]$$
$$= \frac{(n+1)(n+2)}{6}\lambda^2, \qquad \text{(A·3)}$$

the variance can be calculated as

$$\sigma^2 \equiv \frac{(n-1)(n+2)}{18}\lambda^2. \qquad \text{(A·4)}$$

As a next step, let us consider that N random variables $L_1, L_2, \ldots, L_N$ with the same $P(L)$ and the same average of (A·1) exist. In our problem, N is the number of grains (all with the same grain size) in a specimen. The central limit theorem in statistics shows that when N is much larger than unity, the difference between $\langle L\rangle$ in eq. (A·1) and the sample average defined as $(L_1 + L_2 + \ldots + L_N)/N$ obeys a normal distribution function with the average zero and the variance σ^2/N. For example, if an UFG specimen with $d = 100\,\text{nm}$ ($n = 10$ for $\lambda = 10\,\text{nm}$) has a volume of $1\,\text{mm}^3$, the number of grains in the specimen is approximately $N \approx 10^{12}$. Therefore, the standard deviation (square root of the variance) can be calculated from eq. (A·4) as $(\sigma^2/N)^{1/2} \approx 2.4 \times 10^{-6}\lambda$. Since this value is much smaller than $\langle L\rangle = 4\lambda$ from eq. (A·1), the normal distribution of the sample average is highly concentrated around $\langle L\rangle$ and by far the most probable value.

REFERENCES

1) S. Cheng, J. A. Spencer and W. W. Milligan: Acta Mater. **51** (2003) 4505–4518.
2) A. H. Chokshi, A. Rosen, J. Karch and H. Gleiter: Scr. Metall. **23** (1989) 1679–1684.
3) T. G. Nieh and J. Wadsworth: Scr. Metall. Mater. **25** (1991) 955–958.
4) G. E. Fougere, J. R. Weertman, R. W. Siegel and S. Kim: Scr. Metall. Mater. **26** (1992) 1879–1883.
5) R. O. Scattergood and C. C. Koch: Scr. Metall. Mater. **27** (1992) 1195–1200.
6) C. C. Koch and J. Narayan: Mater. Res. Soc. Sym. Proc. **634** (2001) B5.1.1.
7) S. Takeuchi: Scr. Metall. Mater. **44** (2001) 1483–1487.
8) J. Schiotz and K. Jacobsen: Science **301** (2003) 1357–1359.
9) H. Conrad and K. Jung: Mater. Sci. Eng. A **391** (2005) 272–284.
10) G. J. Fan, H. Choo, P. K. Liaw and E. J. Lavernia: Mater. Sci. Eng. A **409** (2005) 243–248.
11) C. E. Carlton and P. J. Ferreira: Acta Mater. **55** (2007) 3749–3756.
12) R. J. Asaro, P. Krysl and B. Kad: Phil. Mag. Lett. **83** (2003) 733–743.
13) R. J. Asaro and S. Suresh: Acta Mater. **53** (2005) 3369–3382.
14) B. Zhu, R. J. Asaro, P. Krysl and R. Bailey: Acta Mater. **53** (2005) 4825–4838.
15) V. Yamakov, D. Wolf, M. Salazar, S. R. Phillpot and H. Gleiter: Acta Mater. **49** (2001) 2713–2722.
16) V. Yamakov, D. Wolf, S. R. Phillpot, A. K. Mukherjee and H. Gleiter: Nature Mater. **1** (2002) 45–49.
17) D. A. Hughes and N. Hansen: Acta Mater. **48** (2000) 2985–3004.
18) N. Hansen, X. Huang and D. A. Hughes: Mater. Sci. Eng. A **317** (2001) 3–11.
19) M. Zhao, J. C. Li and Q. Jiang: J. Alloys Compd. **361** (2003) 160–164.
20) Q. Wei, S. Cheng, K. T. Ramesh and E. Ma: Mater. Sci. Eng. A **381** (2004) 71–79.
21) S. Cheng, E. Ma, Y. M. Wang, L. J. Kecskes, K. M. Youssef, C. C. Koch, U. P. Trociewitz and K. Han: Acta Mater. **53** (2005) 1521–1533.
22) A. S. Argon and S. Yip: Phil. Mag. Lett. **86** (2006) 713–720.
23) H. Petryk and S. Stupkiewicz: Mater. Sci. Eng. A **444** (2007) 214–219.
24) J. C. M. Li: Trans. Metall. Soc. AIME **227** (1963) 239–247.
25) A. Mascanzoni and G. Buzzichelli: Phil. Mag. A **22** (1970) 857–860.
26) L. E. Murr: Metall. Mater. Trans. A **6** (1975) 505–513.
27) F. Spaepen and D. Y. W. Yu: Scr. Mater. **50** (2004) 729–732.
28) M. Dao, L. Lu, R. J. Asaro, J. T. M. De Hosson and E. Ma: Acta Mater. **55** (2007) 4041–4065.
29) J. Weertman and J. R. Weertman: *Elementary Dislocation Theory*, (Macmillan, New York, 1964).
30) F. R. N. Nabarro: *Theory of Crystal Dislocations*, (Oxford University Press, Oxford, 1967).
31) J. P. Hirth and J. Lothe: *Theory of Dislocations*, 2nd ed., (John Wiley and Sons, Inc., New York, 1982).
32) N. Krasilnikov, W. Lojkowski, Z. Pakiela and R. Valiev: Mater. Sci. Eng. A **397** (2005) 330–337.
33) J. Chen, L. Lu and K. Lu: Scr. Mater. **54** (2006) 1913–1918.
34) Y. F. Shen, L. Lu', Q. H. Lu, Z. H. Jin and K. Lu: Scr. Mater. **52** (2005) 989–994.
35) A. S. Khan, Y. S. Suh, X. Chen, L. Takacs and H. Zhang: Int. J. Plasticity **22** (2006) 195–209.
36) M. A. Haque and M. T. A. Saifp: Scr. Mater. **47** (2002) 863–867.
37) O. Nijs, B. Holmedal, J. Friis and E. Nes: Mater. Sci. Eng. A, (2008) in press.
38) F. Dalla Torre, H. Van Swygenhoven and M. Victoria: Acta Mater. **50** (2002) 3957–3970.
39) Y. M. Wang and E. Ma: Appl. Phys. Lett. **83** (2003) 3165–3167.
40) R. Schwaiger, B. Moser, M. Dao, N. Chollacoop and S. Suresh: Acta Mater. **51** (2003) 5159–5172.
41) Y. M. Wang and E. Ma: Mater. Sci. Eng. A **375–377** (2004) 46–52.
42) J. May, H. W. Höppel and M. Göken: Scr. Mater. **53** (2005) 189–194.
43) F. Dalla Torre, P. Spätig, R. Schäublin and M. Victoria: Acta Mater. **53** (2005) 2337–2349.
44) F. H. Dalla Torre, E. V. Pereloma and C. H. J. Davies: Acta Mater. **54** (2006) 1135–1146.
45) L. Hollang, E. Hieckmann, D. Brunner, C. Holste and W. Skrotzki: Mater. Sci. Eng. A **424** (2006) 138–153.
46) Y. M. Wang, A. V. Hamza and E. Ma: Acta Mater. **54** (2006) 2715–2726.
47) M. Dwass: *Probability: Theory and Alppications*, (W. A. Benjamin, Inc., New York, 1970).